Using Surface Evolver to measure pressures and energies of real 2D foams submitted to quasi-static deformations

Marco Mancini, Elhadji Mama Guène, Jérôme Lambert, Renaud Delannay

Using Surface Evolver to measure pressures and energies of real 2D foams submitted to quasi-static deformations

Marco Mancini[a], Elhadji Mama Guène[b,c], Jérôme Lambert[b,1,*], Renaud Delannay[b]

[a] *LUTH, Observatoire de Paris, CNRS UMR 8102, Université Paris-Diderot 5 place Jules Janssen 92195 Meudon cedex*
[b] *IPR Université Rennes 1 - UMR CNRS 6251 Bâtiment 11A - Campus Beaulieu 35042 Rennes cedex France*
[c] *African Institute for Mathematical Sciences (AIMS) KM 2, Route de Joal (Centre IRD Mbour) B.P. 1418 Mbour Senegal*

Abstract

Static 2D foams have the interesting property that their energy is measurable by summing up the total length of their films, so that a simple optical picture of a 2D foam should enable measurement of its energy and other quantities such as its bubbles' pressures. This operation is of course unrealisable in most experiments since the optical resolution limits the accuracy of length measurements. Here we show that using image analysis tools alongside an iterative procedure based on the Surface Evolver (1) to analyse optical images of a 2D foam we are able to measure accurately its energy and its bubbles' pressures up to a single multiplying factor. We validate this procedure by comparing experimental measurement of work and pressure on a 2D foam experiencing a quasi-static localised deformation with the energy and pressures computed using our procedure.

Keywords: 2D foam reconstruction, Surface Evolver, 2D foam rheology

*Corresponding author
Email address: jerome.lambert@univ-rennes1.fr (Jérôme Lambert)
[1]Tel: +33223236068 - Fax: +33223236717

1. Introduction

Foams are usually considered as good model systems for the study of complex fluids, because both their intermediate structure, the bubble, and the events that are responsible for their plasticity are well identified: they consist in an exchange of neighbors between bubbles and are called T1s (2; 3). Foams that are placed between two parallel plane surfaces in order to obtain only one layer of bubbles are called 2D foams and offer the possibility to observe all their bubbles and T1s, which consist in this particular case in the exchange of neighbors between four bubbles. Many studies have been dedicated to 2D foams in the last 20 years because of the possibility they offer to compare numerical and actual experiments that show features which may occur in more complex, or less accessible, situations like, for example, 3D foams. For example, many authors have worked on 2D foam rheology for different kinds of set-ups and flow regimes, and have compared experiments with real foams and simulated foams (see (4) and references therein).

Indeed, one of the reasons why 2D foams are particularly studied is the fact that their structure is visible and that it is possible to observe directly any change that occurs under strain. In addition, it is possible, in principle, to derive the energy of static foams from their structure up to a single factor that accounts for the physico-chemistry since their energy is proportional to the total surface area of their films, and one may thus obtain obtain informations about the local stress in static and moving foams. One may expect to extend this procedure to quasi-static foams where the films experience slow enough motion for the pressure drop induced by viscosity in the Plateau borders to be negligible compared to the Laplace pressure drop.

In principle, it is thus possible to measure precisely the total length of the films and their curvatures on high resolution images of 2D foams using standard image analysis tools. This will lead to the measurement of the pressure inside each bubble and to the measurement of the total energy of the foam. However this process may be tedious and difficult to achieve when imaging a foam containing a large number of bubbles and when one wishes to follow its dynamics. The experimental apparatus required for this kind of measurement is expensive and both the computation time needed to perform the image analysis and the storage of the images are costly.
We show here that an excellent measurement of the characteristics of a 2D foams, as well as of their dynamics is easily achievable using standard res-

olution images coupled with the Surface Evolver (SE) software (1). Indeed a mere standard image analysis is not enough on standard size images: A normal image is 770×550 pixels large and contains around 2000 bubbles (for a foam filling the image). Hence the average length of a film is around 10 pixels. This is too small to obtain a good precision measurement of the film lengths and their curvatures using standard image analysis tools.
One way of achieving the reconstruction of the structure of a 2D foam from a standard size optical image, hence of obtaining a precise measurement of its total energy and of the pressures inside the bubbles, is to measure accurately the positions of the vertices inside the foam and use them as inputs in the mechanical equilibrium equations that govern the curvature of the edges of bubbles. This eventually comes to solving iteratively a linear system for the films' curvatures inside the foam starting from straight films (3; 5). By successive refinements, one may adjust the curvatures of the films and deduce the pressure drop between neighboring bubbles. This method is centered on film curvatures, hence it deals with a large number of variables. An equivalent of this procedure can be achieved using the Surface Evolver (SE) software devised by Ken Brakke to compute stable structures based on surface minimization (1; 6): this software performs the total length's minimization of the structure of a 2D foam given some constraints: Usually the areas (2D foams) or volumes (3D foams) are fixed and the vertices moved in order to minimise the total length (2D) or area (3D) of the foam. This software has been widely used by several authors working on 2D foams (see e.g. (2; 3)) as well as on 3D foams (7; 8; 9) to simulate various aspects of foam behaviour, like coarsening and rheology (4) and compare them to experiments with liquid foams. Here we use SE to reconstruct the structure of foams starting from experimental images. The areas or volumes that are used as constraints are determined experimentally from the optical images or simply assuming that edges are straight or faces are pyramids. Hence, while SE provides a very accurate way of equilibrating a structure whose topology is known, the fact that the exact areas or volumes are not measurable induces a mismatch between the equilibrated numerical structure and the experimental image it reproduces. For example, in a 2D foam, the area of each bubble in the equilibrated structure will match the area of the inscribed polygon of the SE input file, but not the area of the bubble on the optical image. This limits the accuracy of the determination of the curvatures of the bubbles' edges and hence the accuracy of the pressure that can be measured.

The aim of this article is to propose here an improvement of the latter method that also uses SE. It consists in running SE several times while adjusting the usual constraint on fixed bubble areas for the area of the inscribed polygon to match its experimental measurement. Hence we apply a feedback loop on the length minimization procedure performed by SE in order to converge iteratively towards an accurate value of the areas of the bubbles, the "error" signal being related to the area of the inscribed polygon for each bubble. This method, that will be described hereafter, minimizes the number of parameters (one per bubble) that must be set in order for the structure of the foam to be approached starting from the position of its vertices and its topology. It is thus well adapted to large collections of images since it is not time or memory consuming: it is thus possible to follow the dynamics of a 2D foam in the quasi-static regime. In addition this method should be transposable to the reconstruction of 3D foams starting from a method like the one described in Davies et al (9).

We first describe the experimental apparatus used to obtain optical images of a 2D foam experiencing an inhomogeneous quasi-static deformation together with measurements of the pressure inside its central bubble. The quasi-static deformation is a series of cycles of inflation and deflation of a bubble at the centre of the foam. We introduce an image analysis procedure to write a SE input file containing the precise position of the vertices of the foam on an image. We then describe a script that calls the SE software starting from this input file to reconstruct an equilibrated numerical foam using the minimum number of variables in order to obtain a fast convergence. We first check that the equilibrated structure obtained with Surface Evolver maps the optical image of the foam and we show that this mapping is not reliable in order to obtain precise values for the pressures inside the foam. A definitive validation is provided by comparing the dynamics of both numerical and real foams experiencing a quasi-static deformation. This is performed by measuring the pressure inside the inflated bubble for each recorded image and comparing these measurements to the pressure of the same bubble in the equilibrated SE structure. Both pressures differ by a factor that takes into account the contribution of the liquid fraction of the experimental foam. We check that this factor should not vary significantly from a bubble to the other in the foam since the variation of the total energy of the numerical foam that includes this factor is consistent with our estimate of the work done experimentally.

2. Experimental apparatus and method

A 3D monodisperse foam is obtained by bubbling air at constant rate (around 10 mL.min^{-1}) at the base of a column containing a foaming solution. The foaming solution contains 4% volumic fraction of commercial dishwashing liquid "Palmolive" brand) and 10% glycerin. The surface tension of the solution is measured using the pendant droplet method: $\gamma = 26.6 \pm 0.5\,\mathrm{mN.m^{-1}}$. It is possible to tune the liquid fraction by controlling the height of the foam at the top of the column. A few hundred bubbles are extracted from the top of the column by bringing a circular glass plate in contact with this foam. The foam is then squeezed between this plate and another one maintained at a constant distance of 1 mm to form a 2D foam in a glass-glass Hele-Shaw geometry. The typical bubble diameter is then around 5 mm.
The bottom glass plate is pre-drilled in its center with a 1.5 mm diameter hole in order to inflate air inside the foam using a computer controlled syringe pump and to measure the pressure inside the bubble using a differential pressure sensor (precision around 0.2 Pa) as pictured on Fig.1. Gas is injected inside the central bubble at a very slow rate (around 250 μL.min^{-1}) in order for the structure of the foam to be equilibrated only by capillary pressures. This is an idealization since viscous drag may play a role even at slow speed. However, an estimate of the pressure drop induced by the viscous forces exerted on each moving film shows that the influence of viscous drag on their shape is not observable here, whereas the cumulated pressure drop between the central bubble and the atmosphere results in an offset on the pressure measured using a pressure sensor. We will estimate this offset in the validation section. An additional pressure loss will play a role in the offset : it is due to the Poiseuille air flow between the sensor and the bubble. The sign of this offset depends on whether the bubble is being inflated or deflated.

The central bubble is submitted to cycles of slow inflation-deflation. The maximum size of the inflated bubble ranges from 20 to 40 times the average bubble size. For example, Fig.2 shows an experimental 2D foam (20% glycerol, 1097 bubbles, 15 cm diameter) at two different stages of the bubble inflation. In Fig.2a, the central bubble is about the same size as all other bubbles, whereas in fig 2b it is about 23 times as large as the others. The inflating rate is slow enough for the deformation to be quasi-static.
The whole sequence is filmed using a 550×770 pixels camera. The image

acquisition rate is 8 images per second. Between 2000 and 4000 images are recorded for each experiment.

3. Foam reconstruction

3.1. Image analysis

In order to write a SE input file corresponding to a given optical image, one needs to identify each bubble, edge and vertex inside the foam. This is done using common image analysis tools. After converting the image to a binary image, one uses a watershed procedure to label bubbles. A thin-skeleton procedure provides the position of the edges and of the vertices inside the foam. An overlap between the three types of objects enables matching edges with vertices and bubbles with edges. Thus one determines the exact topology of the foam by determining which bubbles share the same edge. SE takes as input the exact position of each vertex. The latter is estimated by computing the position of the centre of mass of each vertex. On the binary images, the vertices all look alike: They are star-shaped sets of 3 to 5 pixels. This enables computing the position of their centre of mass with a precision of the order of a third of the pixel size in both x and y planar directions.
A cycle of bubble inflating/deflating corresponds roughly to 1500 images. We automate the procedure described above in order to write a SE file corresponding to each image and pressure measurement. Let us underline that, at this point, the SE input file merely contains the coordinates of each vertex, which are the most reliable piece of information one can extract from an image, along with the exact topology of the real foam.

3.2. Equilibrating the numerical foam

A way to proceed with the numerical foam equilibration using SE should be to set the vertices to fixed positions and use the standard equilibration procedure under SE by maintaining the vertices fixed throughout the equilibration procedure. However this method may pose convergence problems when some films are very short (e.g. shortly before a T1) and the relative error due to the position of the center of mass of the vertices becomes too important for SE to give a reliable output on the pressures of the bubbles surrounding this short film.
We choose to introduce an alternative way of equilibrating the structure by adding a feedback loop to the procedure based on constant surfaces constraint. We thus keep the advantages of the latter method by setting only

one constraint for each bubble in the foam. But this constraint is fine-tuned after each SE equilibration in order for the area of the polygon whose vertices are the vertices of the bubbles to match with their value deduced from the optical image. Since the positions of the vertices are measured with a good precision on this optical image, the polygon areas are determined rather precisely.
Around ten iterations of area adjustments are needed to obtain an equilibrated numerical structure as close as possible to the real structure as seen on optical images. We first describe the procedure in detail and then the way we compare the successive numerical structures with the real one.

For each bubble i of the SE input file we compute ${a_i}^*$ the area of the polygon the vertices of whose are the bubble's vertices. The goal of the procedure is for each bubble to be mechanically equilibrated whilst its corresponding polygon reaches the target area ${a_i}^*$ that is measured on the initial structure built from the optical image.
Let us write ${A_i}^p$ the area of bubble i before a $p-$th equilibration by SE. At step 0 of the procedure, ${A_i}^0 = {a_i}^*$ for each bubble since the structure of the foam has not been equilibrated yet and since the films are straight lines. Running an equilibration with SE at constant ${A_i}^p$, releases the vertices and leads to a new structure and new values for the polygon areas ${a_i}^{p+1}$. This structure is mechanically equilibrated. The feedback procedure consists in adjusting the constraints ${A_i}^{p+1}$ of the next equilibration to reduce the difference between ${a_i}^{p+2}$ and ${a_i}^*$. To do so, we choose to use a bisection method.

A first step of the bisection method procedure consists in determining a lower A_{im} and an upper boundary for A_{iM} for each bubble i. For each bubble, these two areas lead to values of a_i that bracket ${a_i}^*$. Once A_{im} and A_{iM} are set for each bubble (we give an example for doing so further in the text), the second step consists in using a bisection method to find the experimental areas using the following algorithm for each bubble i ($p = 0$ designates the initial non-equilibrated structure):

$A_i^p = \frac{1}{2}(A_{iM} + A_{im})$
SE equilibration at constant ${A_i}^p$ leads to new ${a_i}^{p+1}$
if ${a_i}^{p+1} - {a_i}^* \geq 0$
then $A_{iM} = {A_i}^p$
else $A_{im} = {A_i}^p$

After p iterations, the relative uncertainty on the value of the areas is indeed of the order of $< \Delta A/A >=< (A_{iM} - A_{im})/A_i > \approx |\delta A|/2^{p+1}/ < A >$ (where $< \cdot >$ designates an average over all the bubbles) as pictured on Fig4a. In the same time, SE ensures that the bubbles' pressures converge as pictured on Fig4b where $< \Delta P/P >=< (P(A_{iM}) - P(A_{im}))/P_i >$. Thus, 10 iterations are enough to reach a 10^{-4} relative precision on the values of A_i, and a 0.2% relative precision on the pressures P_i. The whole procedure is quite fast since it requires $\approx 200\,\mathrm{s}$ to run on a 800 bubbles foam with a 1.6 GHz CPU.
The structures that are obtained using this procedure are thus mechanically equilibrated and seem to be similar to the structures of the foam from which they were originally deduced. We show in the following paragraph that the measurement made on the numerical structures are indeed very similar to experimental measurement that are made independently.

Let us end this description by making two remarks :

- We use a fast way of determining the lower and upper bounds of A_i by deliberately trying to "overshoot" the convergence. A few equilibrations with SE are run after setting the new constraints on A_i as :

$$A_i{}^{q+1} = A_i{}^q - s_q(a_i{}^q - a_i{}^*)$$

  where s_q is an increasing set of positive numbers, that is chosen to force $(a_i{}^q - a_i{}^*)$ to change signs as q increases. We use q rather than p here to stress the difference between this initiation stage, which is only but an example of method to obtain the initial values for A_M and A_m, and the bisection procedure. We set $s_q = q$, which leads to a quick convergence: We obtain values bracketing $\bar{a}_i$ for each bubble with 2 successive iterations, although not in the same order for each bubble. This procedure is run until we obtain for each bubble two successive values of A_i for which the areas of inscribed polygons bracket $a_i{}^*$. The lower and larger areas are named A_{im} and A_{iM}. Let us notice that the number of iterations needed to reach this result for each bubble is observed to be always smaller than 5.

- It may look surprising that the bisection method works so well as if there were only one A_i matching a a_i for each bubble, or that A_i might be an increasing function of a_i, independently of the value of A_j for

neighboring bubbles. The authors are aware of this problem, but it seems that the films in the structures that are studied in this article are close enough to straight films for this approximation to hold. We nevertheless tested this procedure on a more polydisperse foam structure ($\Delta A/ < A >= 3$) where the films were clearly distinct from straight lines. Further work on more complex structures, like very polydisperse foams, might set a limit to the efficiency of the procedure we describe here. Nevertheless, even with the huge size polydispersity that we have here (one very large bubble among small ones), the method works very well.

4. Validation

4.1. Image correlation

A first - although very crude - way to check the validity of the method is to compare the foam structure on both optical and SE images. One may build the latter from the SE file by discretizing the edges with a large number of points, *i.e.* a number larger than the ratio of the maximum edge length to the size of a pixel. Of course this procedure results in a loss of information. Figure 3(a) shows an optical image of a 2D foam containing 1097 bubbles. One may build an image using the SE input file obtained by image analysis, as shown in figure 3(b). After 11 iterations, the reconstructed structure (figure 3(c), obtained using the same procedure) is very close to the original one. A superposition of the three images merged in a RGB image provides a crude means to check this observation, as is shown on figure 5a.
A quantitative analysis of the image matching is performed by measuring the overlap ration between the binary original image after it has been slightly blurred and the successive images built from the SE files (also slightly blurred). In order to do so, we compute the average of the pixel by pixel multiplication of both images. Thus this overlap ratio appears to be the value of the correlation function between both images at frequency zero. The result is pictured on figure 5b. One may understand this result as a way to estimate the accuracy of measurements based on image analysis only: Two SE steps are enough to get the same estimate of the energy as the one that could be obtained by merely counting the number of pixels of edges on an optical image after it has been converted to a binary image. This shows that, whereas the correlation reaches a steady value at the third iteration

(this value depending on the pretreatment of the images, it is of no particular interest), one needs to run more iterations to obtain a good precision in the determination of the areas and pressure.

4.2. Accuracy

In order to obtain an evidence that our procedure may indeed provide quantitative information about the foam, *i.e.* good estimates of pressures or areas of the bubbles, let us first examine the accuracy of the pressures and areas that are measured and then compare them to experimental measurements. It is easy to check when an error occurs in determining the topology and to correct it. Thus, the only source of inaccuracy is the error on the position of the vertices. Errors may occur in the initial position of the vertices as a result of the image analysis process: indeed the latter provides the positions of the vertices with a 0.33 pixel precision in both directions. This error in the input file of course modifies the final areas and pressures after the SE equilibration process. Let us estimate the errors on pressure P_i and area A_i of bubble i by moving *randomly* each vertex in the SE input file of ± 0.33 pixel in x and y directions and measuring the resulting ΔA_i and ΔP_i for each bubble after equilibration. The size of the range in which A variations are very small for both quantities as shown on figure 6 after averaging over all the bubbles for a foam containing 1104 bubbles. The maximum relative error induced by the random displacement of vertices on pressures and areas are 2% and 5% respectively. This can be understood by noticing that, for an average edge length of 10 pixels, the area corresponding to the uncertainty on the position of a vertex is much smaller that the average area of a polygon. A few vertices may experience a 1 pixel displacement but most of them move inside the margin defined by the image analysis step as can be seen on figure 7: the average displacement is around half the margin induced by image analysis. Thus the accuracy on the measurement of the pressures and areas of the procedure is excellent.

4.3. Comparison with experimental measurements

The errors discussed above are relative errors, insensitive to the absolute values of pressure and areas. One must therefore calibrate the scales of pressures and areas. The process is straightforward for areas : the pixel area is easily measurable on optical images using a ruler. As for the pressures,

the pressure sensor provides a good estimate of the pressure P_{Sensor} inside the central bubble (CB), but with an offset the sign of which depends on the direction of the gas flow inside the pipe. This offset is induced by the air flow in the tube : $P_{\mathrm{CB}} = P_{\mathrm{Sensor}} - \Delta P_{\mathrm{flow}}$. Considering the air flow as a Poiseuille flow, one gets :

$$\Delta P_{\mathrm{flow}} = \frac{8\eta Q L}{\pi R^4} \approx 0.7\,\mathrm{Pa}$$

where $\eta = 17.1\,10^{-6}\,\mathrm{Pa.s}$ is the air viscosity, $Q = 250\,\mu\mathrm{L.min}^{-1}$ the flow rate fixed by the syringe pump (positive for the inflating stage, negative for the deflating stage), $L = 120\,\mathrm{cm}$ and $R = 0.75\,\mathrm{mm}$ the length and radius of the tube. As for the air flow in the gap between the two glass plates, it induces a pressure drop that is proportional to h^{-3} in a plane geometry. Since $h = 1$ mm is of the same order of magnitude as R, the pressure drop per unit length inside the cell is approximately 1000 smaller than in the pipe. Thus one can neglect it.

In addition, the relation between the dimensionless numerical pressure P_{num} computed using SE and P_{CB} should be

$$P_{\mathrm{CB}} = a\,P_{\mathrm{num}} + \Delta P_{\mathrm{visc.}}$$

where the offset is now due to the viscous drag exerted on the films and a is a constant pressure. Let us estimate the order of magnitude of $\Delta P_{\mathrm{visc.}}$: Cantat *et al.* (10) show that the pressure drop depends on the orientation of the film with respect to its velocity. Only films perpendicular to the flow will experience a pressure drop. For a typical flow rate of $250\,\mu\mathrm{L.min}^{-1}$, the speed of a film at a typical distance $r = 1.5\,\mathrm{cm}$ of the injection tube is $v \approx 5.10^{-3}\,\mathrm{cm.s}^{-1}$ (for a 20% volumic glycerin solution, this corresponds to a Capillary number $\mathrm{Ca} \approx 2.10^{-6}$). The resulting pressure drop is then of order $3.10^{-2}\,\mathrm{Pa}$ (see (10)), which is less than the resolution we can expect from our equilibration procedure. Hence we won't see any difference between the structure we image and a static one. However this drop may cumulate across the foam to give a measurable pressure drop between the central bubble and the atmosphere. We image foams that are approximately organized as 10 to 20 rings of bubbles around the central bubble. Assuming for sake of simplicity that all the films move at the same speed, this may lead to an average pressure drop of $\Delta P_{\mathrm{visc.}} = \pm 0.3\,\mathrm{Pa}$ depending on the sign of the gas flow

rate. This offset in large enough to modify slightly the value of the pressure inside the central bubble.

The a factor has pressure dimensions and depends on the geometry of the foam and on the surface tension. It might depend as well on the bubble that is under scrutiny. To compute this factor, let us introduce b, the length scale enabling linking SE structures to real ones. The dimensionalized film lengths and bubble areas are :

$$\ell_{ij(d)} = b\,\ell_{ij} \qquad \text{and} \qquad A_{i(d)} = b^2 A_i$$

where ℓ_{ij} is the length of the film that is common to bubbles i and j, and where the (d) subscript stands for a dimensionalized quantity. One may write the relation between the pressure in bubble i and its area in SE :

$$P_i = \frac{\partial E}{\partial A_i}$$

where $E = \sum \ell_{ij}$ is the energy of the foam. Let g be a geometrical factor that describes the shape of a film along its height (we will derive it further). Then the dimensionalized energy and pressures are respectively :

$$E_{(d)} = 2\gamma \sum_{\text{films } \{ij\}} h\,g\,\ell_{ij(d)} = 2\gamma h g b\,E$$

and

$$P_{i(d)} = \frac{\partial E_{(d)}}{h\,\partial A_{i(d)}} = \frac{2\gamma g}{b}\frac{\partial E}{\partial A_i}$$

Comparing the latter equation in the case of the central bubble leads to

$$a = \frac{2\gamma g}{b}$$

One can use a crude model of film shape in order to derive g : Fig. 8 shows a naive shape of a 3D film compared with the idealization of a 2D film. The 3D film is itself idealized for two reasons : first the liquid phase is evenly shared between the top and the bottom ends of the film. This assumption is justified by the fact that the height of the foam is slightly less than the capillary length. The second reason is that we neglect the second curvature radius of the film by considering a straight segment between the

two glass plates. Whilst this is true for a static film, a moving film may possess a second curvature radius to balance the drag force exerted on both its upper and lower ends (see e.g. (11)). However we estimated above that the added pressure increase induced by the drag force on one film is around 0.03 Pa, which is much less than the pressure variations we observe during both inflating and deflating stages. Thus we choose to neglect this second curvature: Films may be considered as static as for their shape. This simple model leads to

$$g = \frac{(\pi - 2)r + h}{h} \tag{1}$$

where r and h are the radius of the Plateau border and the height of the foam respectively.

Thus the relation between the numerical pressure and the pressure recorded by the sensor is :

$$P_{\text{Sensor}} = a\, P_{\text{num}} \pm \Delta P = \frac{2\gamma g}{b} P_{\text{num}} \pm \Delta P$$

where $\Delta P \approx 1.0\,\text{Pa}$ takes into account both sources of pressure drop. The plus or minus sign depends on whether the bubble is inflated or deflated. To determine g (the only unknown quantity in the factor) and ΔP experimentally we compare the dynamics of P_{Sensor} and $\frac{2\gamma}{b} P_{\text{num}}$ for a set of 1500 successive images during the central bubble inflation.

Figure 9 shows the variations of both quantities where P_{num} is now dimensioned : we write $P_{\text{Evolver,wet}} = \frac{2\gamma g}{b} P_{\text{num}} + \Delta P$ and $P_{\text{Evolver,dry}} = \frac{2\gamma}{b} P_{\text{num}} + \Delta P$. Both factors g and ΔP are détermined by the least squares method. One finds that $g = 1.407$ and $\Delta P = .91\,\text{Pa}$ give the best accord between SE and pressure sensor data.

Wet Evolver data and pressure sensor data are well correlated except at the beginning of the inflation sequence (from t=0s to t=50s) and at the beginning of the deflation sequence (from t=255s and 305s) during $\Delta t \approx 55\,\text{s}$ when we suppose that the experimental set-up slowly adapts to the new flow regime. We discuss only the intervals outside this adaptation period in the following paragraphs.

One may see both experimental and numerical pressures vary continuously except when plastic events (T1) occur. These T1 look instantaneous on this figure but a close look at the few points that come immediately after the T1 show that the only discrepancies between the two pressure sets (apart from the initial stage and noise on the Sensor measurements) occur in the

half second following the event. This is due to the fact that most T1 occur near the central bubble and that the structure is not mechanically equilibrated anymore. Thus an optical image cannot provide coherent data to build a mechanically equilibrated SE structure. T1 characterization using the method introduced here will be discussed in (12).
By comparing both numerical and experimental curves during inflation and deflation, the value of ΔP is found to be around $\pm.9\,\mathrm{Pa}$, with a mere sign change between both phases. This value is close to the theoretical prediction taking into account the Poiseuille pressure drop and the viscous drag on films.

In order to prove that g is indeed a constant throughout the foam, and may be considered as a manifestation of the liquid fraction, we compare the experimental work done to change the shape of the foam with its energy $\Delta E(t)$ computed by SE and and dimensioned with the constants introduced before. In the quasi-static regime and in the absence of $T1$ events, both quantities must be equal. This writes

$$\Delta W(t) = \int_0^t (P_{CB} - P_{ext})\mathrm{d}A_{CB} = \Delta E(t)$$

While the work depends only on the area of the central bubble and on the difference $P_{CB} - P_{ext}$, the energy is influenced by the whole structure of the foam. If a and thus g were to vary in the foam, this would reflect on the energy, but not on the work. Figure 10 shows that the average values of ΔE and δW are indeed equal when $g = 1.4$. This validates the hypothesis that g is a geometrical factor accounting for the shape of the films.
From the expression (1) of g written above, it is then possible to derive the liquid fraction of the foam (assuming the bubbles are circles of radius $\ell \approx 2.5$ mm): one finds $\phi_\ell \approx 5\%$, which is a credible value given the way the foam was made.

5. Conclusion

In this paper we show a new way of measuring the total energy along with each bubble's pressure of a 2D foam experiencing quasi-static deformation by combining image analysis tools with the SE software. The method relies on a determination of the position of the vertices and of the topology of a foam on the one hand, and on the use of SE to build an equilibrated structure starting with these data on the other hand. Other means of equilibrating the

structure using SE can be employed but the method introduced here favors the least number of variables. This was useful in this study because of the great number of images to be analyzed. But it should also be useful for future studies on $3D$ foams. Optical tomography tools have been used first by Monnereau *et al* to observe a few tens of bubbles in the bulk of a coarsening foam (7). The same authors were able to rebuild the same mechanically equilibrated structure using SE to characterize the coarsening process (8). X-ray tomography now makes it possible to observe larger numbers of bubbles in quasi-static liquid foams (e.g. see (13)). But the reconstruction of such structures under SE requires an automated procedure. Davies *et al* (9) have recently demonstrated a way to build the latter and to obtain an SE equilibrated structure close to the experimental foam structure. The procedure described in the current paper could be applied to 3D structures to obtain a better description of the pressures inside the bubbles by including a feedback control parameter to better adjust the volume of the SE reconstructed bubbles to the experimental ones. This might be especially interesting since most of the imaging methods in 3D produce images where only the vertices are clearly visible, and where the films are often faint or even invisible. Such a method would certainly greatly improve the analysis of 3D foam structures since it would not rely on a precise observation of the films.
The current paper opens the possibility to analyze a great number of quasi-static experiments and to measure the distribution of pressures inside 2D foams since the film curvatures could hardly be measured using standard image analysis tool. In future studies, we will analyse the global behavior of a foam under many cycle of inflation and deflation of the central bubble as well as the energy and range of a $T1$, which has been numerically analyzed by Cox *et al.*(14).

6. Acknowledgements

The authors thank the "Region Bretagne" for awarding a ARED grant to this project. They also gratefully thank Isabelle Cantat, Simon Cox, Benjamin Dollet and François Graner for numerous and useful discussions, Janine Émile and Alain Faisant for their kind technical assistance at different stages of the experiment.

[1] K. Brakke, The surface evolver, Experimental Mathematics 1 (2) (1992) 141–165.

[2] D. Weaire, S. Hutzler, The physics of Foams, Oxford University Press, 1999.

[3] I. Cantat, S. Cohen-Addad, F. Elias, F. Graner, R. Höhler, O. Pitois, F. Rouyer, A. Saint-Jalmes, Les mousses, structure et dynamique, Paris, France:Belin . English translation 'Foams: structure and dynamics', R. Flatman (trans.), (ed. SJ Cox). OUP, 2010.

[4] A. Kabla, G. Debregeas, Quasi-static rheology of foams. part 1. oscillating strain, Journal of Fluid Mechanics 587 (2007) 23–44. doi:10.1017/S0022112007007264.

[5] B. Foley, Reconstruction of two-dimensional foams, Master's thesis, Trinity College, Dublin (2001).

[6] K. Brakke, http://www.susqu.edu/facstaff/b/brakke/evolver/.

[7] C. Monnereau, M. Vignes-Adler, Dynamics of 3d real foam coarsening, Physical Review Letters 80 (23).

[8] C. Monnereau, M. Vignes-Adler, N. Pittet, Coarsening of a three-dimensional reconstructed foam under surface evolver, Philosophical Magazine Part B 79 (8) (1999) 1213–1222. arXiv:http://www.tandfonline.com/doi/pdf/10.1080/13642819908218316, doi:10.1080/13642819908218316.
URL http://www.tandfonline.com/doi/abs/10.1080/13642819908218316

[9] I. T. Davies, S. J. Cox, J. Lambert, Reconstruction of tomographic images of dry aqueous foams, Colloids and Surfaces A: Physicochemical and Engineering Aspects 438 (2013) 33 – 40. doi:http://dx.doi.org/10.1016/j.colsurfa.2013.01.051.
URL http://www.sciencedirect.com/science/article/pii/S0927775713000782

[10] I. Cantat, N. Kern, R. Delannay, Dissipation in foam flowing through narrow channels, EPL (Europhysics Letters) 65 (5) (2004) 726.

[11] P. Grassia, G. Montes-Atenas, L. Lue, T. Green, A foam film propagating in a confined geometry: Analysis via the viscous froth model, The European Physical Journal E 25 (1) (2008) 39–49. doi:10.1140/epje/i2007-10262-8.
URL http://dx.doi.org/10.1140/epje/i2007-10262-8

[12] E. M. Guène, M. Mancini, J. Lambert, R. Delannay, Cycles of deformation in a 2d foam, to be published.

[13] J. Lambert, I. Cantat, R. Delannay, A. Renault, F. Graner, J. A. Glazier, I. Veretennikov, P. Cloetens, Extraction of relevant physical parmeters from 3d images of foams obtained by x-ray tomography, Colloids and Surfaces A: Physicochem. Eng. Aspects 263 (2005) 295–302.

[14] S. J. Cox, F. Graner, M. F. Vaz, Screening in dry two-dimensional foams, Soft Matter 4 (2008) 1871–1878. doi:10.1039/B802792G.
URL http://dx.doi.org/10.1039/B802792G

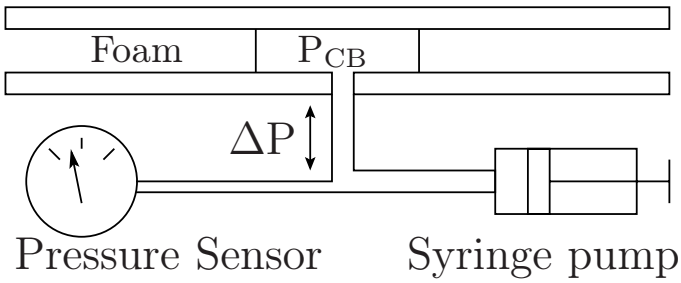

Figure 1: Hele-Shaw cell and pressure circuit involving the syringe pump, the central bubble and the pressure sensor.

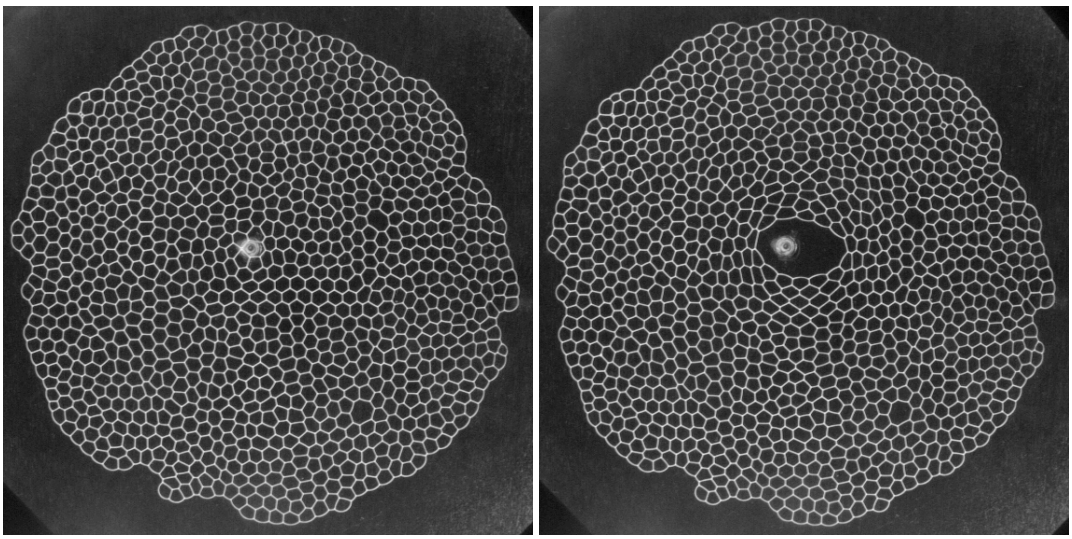

Figure 2: Experimental 2D foam (f2) at two different stages of the bubble inflation. a) Initial stage before inflation. b) Central bubble is about 23 times as large as the average bubble size.

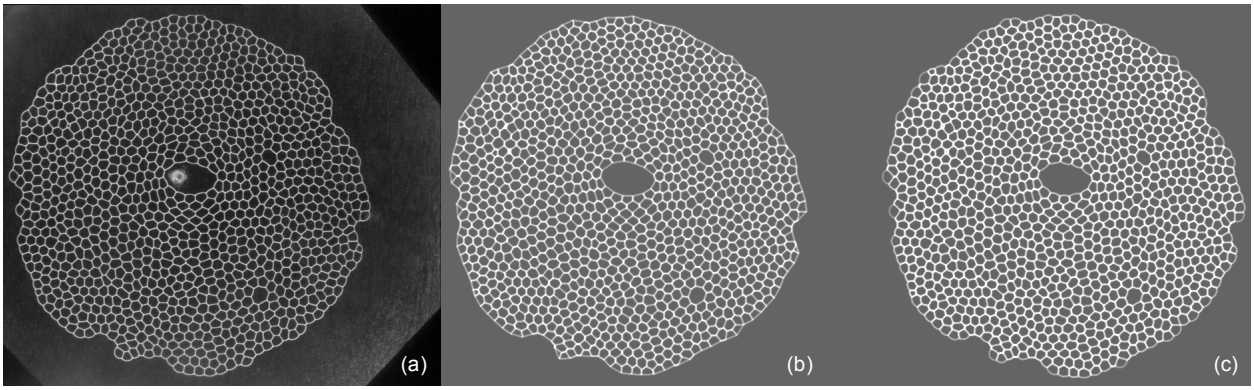

Figure 3: a) Optical image of a 1097 bubbles 2D foam. b) Image built from SE input datas obtained by analysing (a). Notice the edges are straight lines. c) Image built from SE output file after 11 iterations of area adjustments.

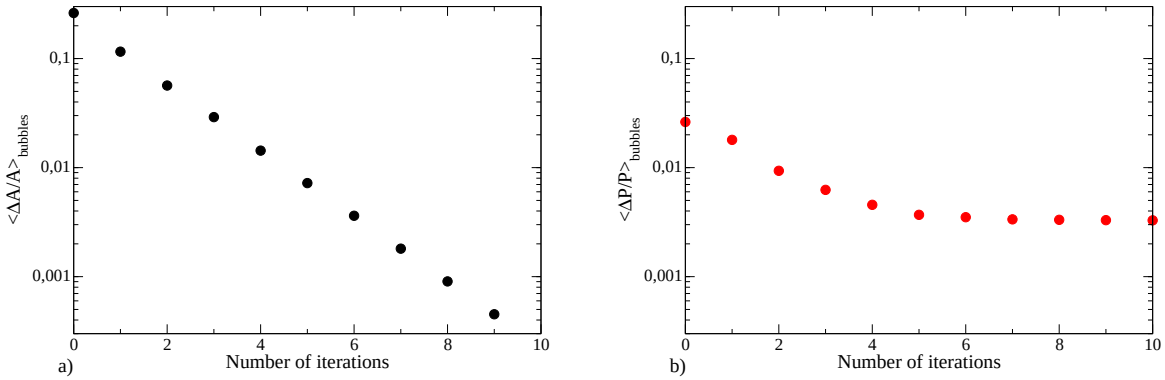

Figure 4: a) Average relative error on bubble area vs. number of iterations of the bisection procedure. b) Average relative error on bubble pressure vs. number of iterations.

(a)

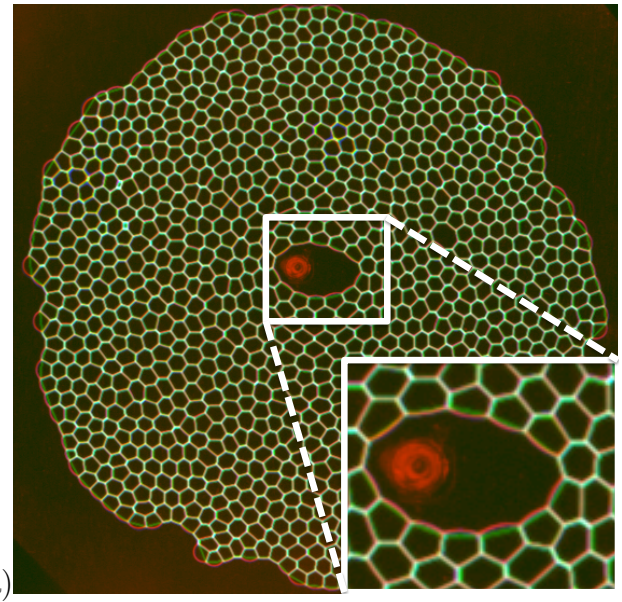

(b)

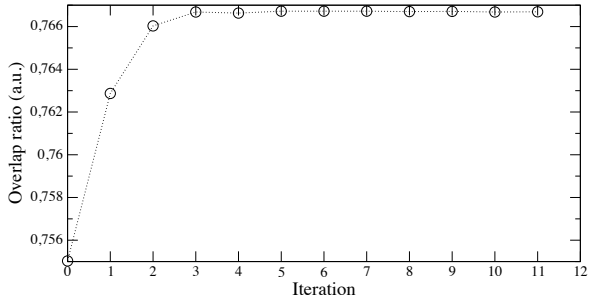

Figure 5: (a) :RGB image obtained by merging different reconstructions of the same foam. Red: Optical image. Green: SE input file. Blue: SE output file after 11 iterations. The insert pictures a detail of the image after zooming in. (b): Overlap ratio between the optical gray-level image and successive images built after n iterations. Iteration 0 stands for the input SE file built using image analysis.

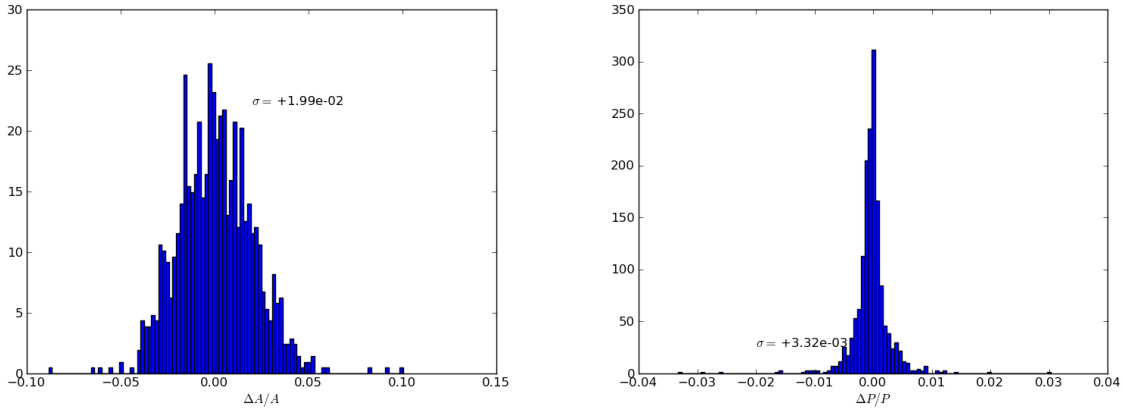

Figure 6: Left : histogram of the relative error on the final value of A_i induced by a random displacement of the vertices in the SE input file. Right : same for p_i.

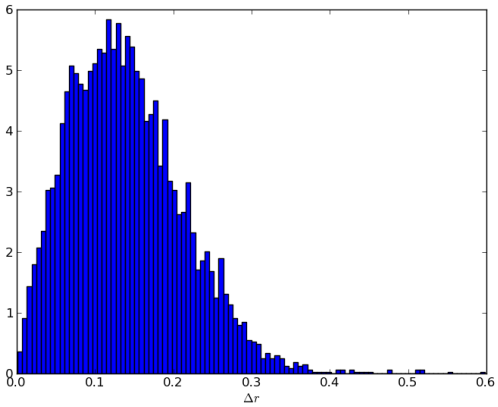

Figure 7: histogram of displacements r_i of vertices induced by the SE equilibration process after 11 iterations.

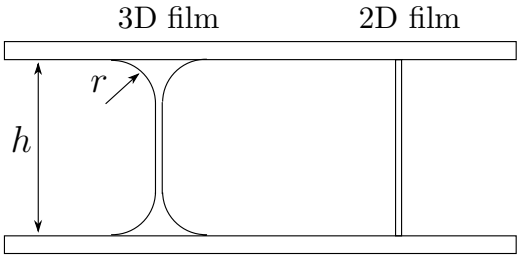

Figure 8: 3D and 2D films.

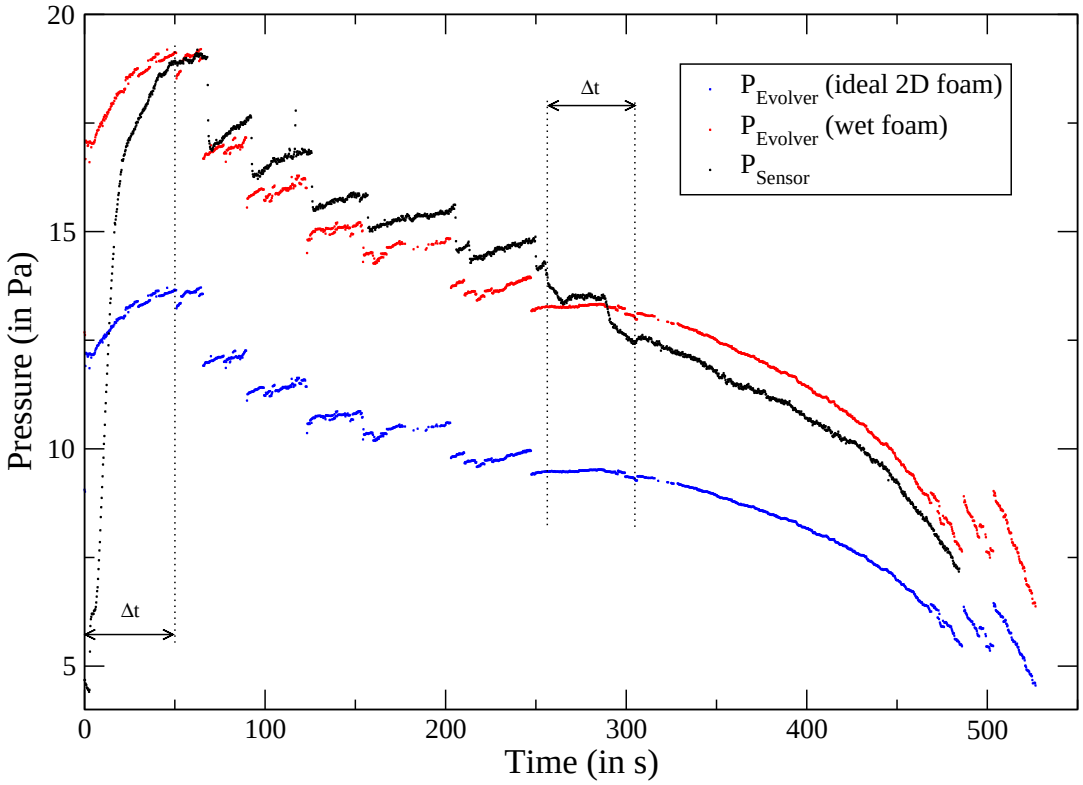

Figure 9: P vs. time for foam 1. Red dots : pressure computed by evolver. Green dots : same pressure multiplied by g. Blue dots : P on the pressure sensor. Δt is the time range during which the experimental set-up is adapting.

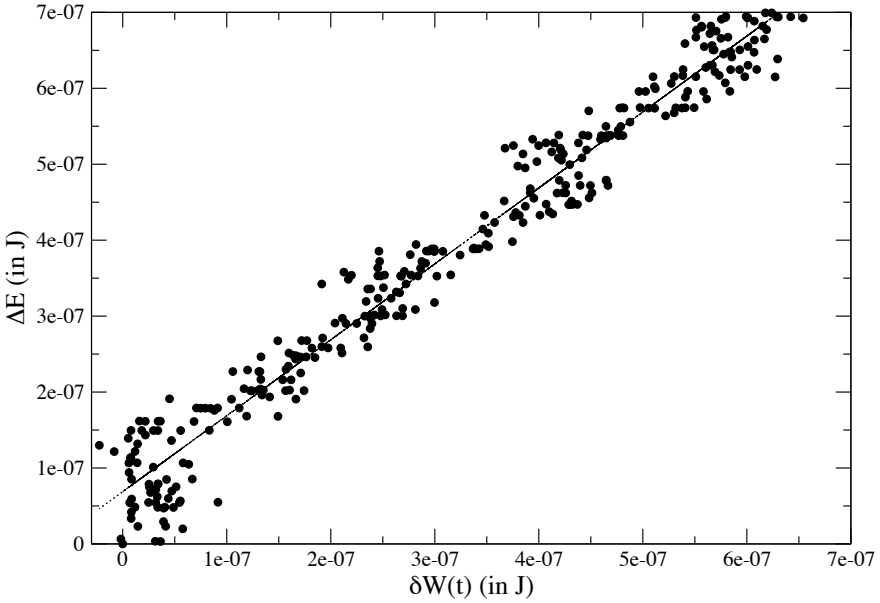

Figure 10: Energy computed using SE vs. work measured by the pressure sensor. Continous line has slope 1.